Terahertz Emission Mechanisms in III–V Semiconductors: The Influence of Isoelectronic Dopants

Rajeev N. Kini and C. P. Vaisakh

Abstract The generation of terahertz (THz) radiation by ultrafast optical excitation of III–V semiconductors has been studied extensively in the last three decades. One of the widely used THz sources/detectors is photoconductive antennas (PCAs) based on low-temperature grown GaAs (LT-GaAs). These PCAs have acted as reliable table-top sources of THz radiation required for different applications ranging from spectroscopy to imaging. THz radiation is generated from these semiconductors by transient photocurrents or by the nonlinear optical phenomenon. In the case of low-bandgap semiconductors, like InAs or GaSb, THz emission is mainly due to transient photocurrents. The transient photocurrent arises due to the built-in surface field or due to the difference in the mobility of electrons and holes generated by the intense laser pulse. III–V semiconductors doped with isoelectronic elements like bismuth have shown interesting properties like giant bandgap bowing, (e.g., 80–90 meV/% of Bi in GaAsBi), increase in hole concentration, and giant spin-orbit bowing. In this chapter, we discuss the effect of Bi incorporation on the THz emission and the mechanisms responsible for THz phenomena in two typical III–V semiconductors, viz. GaAs and GaSb. Even though the THz emission mechanism in these two alloys is different, an enhancement in the THz emission efficiency in both the alloys with increased Bi concentration has been reported. We discuss potential applications of these III–V: Bi alloys.

1 Introduction

Semiconductors hold a special place in terahertz science and technology. They are among the crucial components of terahertz technology ever since the beginning of investigations in this spectral realm. Ultrafast optical excitation of semiconductors

R. N. Kini (✉) · C. P. Vaisakh
Indian Institute of Science Education and Research Thiruvananthapuram (IISER-TVM), Maruthamala PO, Vithura, Thiruvananthapuram, Kerala, India
e-mail: rajeevkini@iisertvm.ac.in

C. P. Vaisakh
e-mail: vaisakhjayadevan@iisertvm.ac.in

© Springer Nature Singapore Pte Ltd. 2020
A. Biswas et al. (eds.), *Emerging Trends in Terahertz Solid-State Physics and Devices*,
https://doi.org/10.1007/978-981-15-3235-1_11

is one of the most popular techniques used to produce terahertz (THz) radiation in table-top spectroscopic systems of the day. A large number of II–VI and III–V semiconductors emit THz radiation upon femtosecond optical excitation due to various physical mechanisms. Studying the THz emission from these materials not only reveals the emission mechanisms but also guides the search for efficient broadband sources of THz radiation. In this chapter, we discuss the influence of isoelectronic alloying of III–V semiconductors in the THz emission phenomenon.

2 THz Emission from Semiconductors

Femtosecond lasers deliver extraordinary optical energy, setting forth interesting processes in materials. Terahertz emission from semiconductors relies on the transient phenomenon (fs-ps) powered by ultrafast optical pulses. It either takes a nonlinear optical route or a transient current route. The nonlinear optical route relies on a process called optical rectification (OR). OR leads to rapid variation in the electric polarization in the semiconductor crystal, and the time-varying polarization acts as the source of THz radiation [1].

$$P_i^{\{2\}}\left(\omega = \omega_p - \omega_q\right) \approx \varepsilon_o \sum_{jk} \sum_{pq} \chi_{ijk}^{\{2\}}\left(\omega = \omega_p - \omega_q; \omega_p, \omega_q\right) E_j\left(\omega_p\right) E_k\left(\omega_q\right) \quad (1)$$

Here, $P_i^{\{2\}}$ is the second-order polarization in the material, $\chi_{ijk}^{\{2\}}$ is the susceptibility tensor and $E(\omega)$ is the electric field of the excitation wavelength. The III–V semiconductor systems like GaAs, InP, GaP, InAs, and II–VI systems like ZnTe, CdTe display broadband THz emission via OR. Like most other nonlinear processes, OR is subject to phase-matching condition and depends on the orientation of crystal axis with respect to the optical polarization of the excitation light. The THz emission could happen through a second-order nonlinear phenomenon in the bulk of the semiconductor and is called the bulk OR. Besides, terahertz radiation could also emerge by a third-order nonlinear process taking place at the semiconductor surface. This phenomenon is called the surface field-induced OR. The femtosecond excitation of the semiconductor generates electron-hole pairs near the surface. The photocarriers undergo drift and diffusion near the surface, constituting transient currents. The strength and nature of transient currents depend on the material system and the photon energy. These transient currents with characteristic subpicosecond lifetimes act as a source of THz radiation.

Semiconductor surfaces host unique energy states called surface states [2, 3]. The surface states play a vital role in the electrical behavior of semiconductors. Several experiments have demonstrated localization of surface states to a narrow band near the mid-bandgap. Hence, it is safe to assume that the surface Fermi level is close to the mid-bandgap. However, in the bulk interior, the Fermi level could be away from the mid-bandgap, and parameters like doping density and donor/acceptor

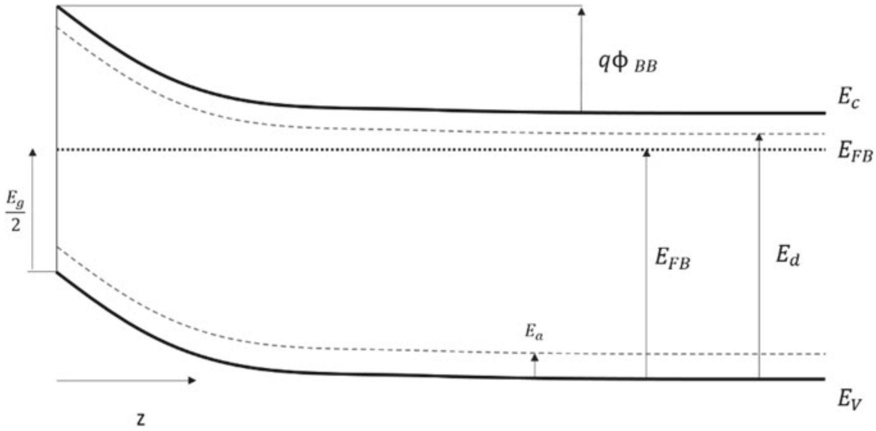

Fig. 1 Band bending at the surface of an *n*-doped semiconductor, which has a bandgap of E_g and whose Fermi level is E_{FB} away from the valance band edge E_V. E_a and E_d represent the position of acceptor and donor levels, respectively, above E_V. The quantity $q\phi_{BB}$ represent the maximum extent of band bending (at the surface) measured from the conduction band edge E_c in bulk

levels determine its position. Due to this, there is a mismatch between the Fermi levels at the bulk and the surface. This mismatch leads to band bending, charge separation, and establishment of the electric field near the surface (depletion region). This phenomenon is called the Fermi-level pinning [2] (Fig. 1).

Ultrafast excitation of the semiconductor surface introduces new carriers in the depletion region, and these carriers accelerate due to the surface electric field. These transient drift photocurrents lead to radiation in the THz frequency range. Wide-bandgap semiconductors like GaAs and InP have higher Fermi-level mismatch and stronger surface fields. Hence, drift currents constitute the prominent emission mechanism. Drift currents form the basis of popular THz source called the photoconductive antenna (PCA). PCAs are made using wideband semiconductors with biased electrodes on the surface where the external electric field drives the drift photocurrent. PCAs, compared to bare surface emitters, offer better flexibility in terms of dipole strength, dipole orientation, spectral tunability, etc.

However, low-bandgap materials do not form strong surface fields. InAs, which is a low-bandgap material, shows the highest amplitude THz emission among III–V semiconductors at 800 nm excitation, and the emission is due to carrier diffusion. In a low-bandgap material that has a short absorption length at 800 nm, when excited with an ultrafast near-infrared (NIR) pulse, a dense pool of hot carriers is created close to the surface. The gradient in carrier density between the bulk and surface drives the diffusion of carriers into the bulk. The hole has a higher effective mass and lower mobility compared to electrons. Hence, the inhomogeneous carrier distribution created by ultrafast optical excitation evolves with a net movement of electrons toward

the bulk. This is called the photo–Dember effect. The transient diffusion current thus generated results in THz emission. Carriers attain high excess kinetic energy and carrier temperature in lower-bandgap materials, making diffusion stronger in them [4].

Drift and diffusion photocurrents coexist in semiconductor systems. However, their relative and absolute strengths depend on many factors, including the bandgap, the position of satellite valleys, mobility, doping density, pump photon energy, etc. Guessing the THz emission mechanisms in a semiconductor system is not easy, as one needs to consider a large number of factors that are at play. For instance, when excited with ultrafast pulses with photon energy ~1.5 eV (λ ~ 800 nm), GaAs with a bandgap, E_g of ~1.42 eV, is a surface field-assisted drift current emitter [5]. On the other hand, studies have shown GaAs transforming into a diffusion emitter when excited at 3.1 eV due to high carrier excess energy [4]. Following this reasoning, one might be tempted to conclude that pumping a system with higher photon energy would force stronger diffusion leading to the photo–Dember effect. However, in the case of InAs (E_g ~ 0.35 eV), pumping with photon energies above ~1.6 eV decreases photo–Dember emission. When excited high up to the conduction band, electrons encounter an increased probability of scattering to the low-mobility satellite valleys [6]. Similar reasoning explains the higher photo–Dember THz emission from InAs compared to the InSb at 1.5 eV excitation, even though InSb has a lower bandgap [7].

Similarly, one would also expect heavy doping as a way to create a higher surface field and leading to higher drift currents. Even though high doping density enhances the field strength, the depletion region becomes very narrow, and hence a large fraction of photocarriers are generated outside the depletion region where there is no field to accelerate the charges. Moreover, the increased screening [8, 9] and high carrier–carrier scattering [10] sharply reduced the THz emission efficiency at high doping levels.

The excitation density of the pump beam is a vital factor in determining the emission mechanism. Let us look at THz emission from InAs. At low intensities, the THz emission happens via the photo–Dember effect [11]. However, at higher fluence, the surface field-assisted OR takes over as the dominant mechanism [12]. Moreover, the drift and diffusion currents tend to saturate at higher fluences (photocarrier–carrier density). The nonlinear phenomenon, on the other hand, might get stronger and show saturation only at much higher excitation densities.

In short, the THz emission from semiconductors is a complex phenomenon that cannot be easily generalized. Multiple emission mechanisms can coexist and compete in a single material system. One has to study the physical system and THz emission carefully to elucidate the underlying emission mechanisms. Such investigations are vital in the pursuit of the identification and design of efficient broadband sources of THz radiation, which have the potential for spectroscopic and technological applications.

3 Isoelectronic Doping

Alloying is a common technique used to tailor the optoelectronic properties of a semiconductor so that it fits the desired application. The process involves the introduction of new isoelectronic elements into the host material. Various isoelectronic species that have characteristics like atomic radii, ionicity, and electronegativity, similar to the host, are preferred. However, exceptions to this also exist. Isoelectronic alloying in III–V semiconductors is one of the heavily investigated areas of semiconductor sciences in the past decades [13, 14]. Such processes often drastically alter the structural, optoelectronic, and transport properties of the parent material. The interest in these alloys is two-fold: scientific curiosities on the nature of perturbations that come along with alloying as well as rich and diverse applications these alloys potentially hold.

The introduction of isoelectronic species perturbs the host semiconductor bandstructure. As mentioned earlier, alloying is a tool to *tune* several material parameters. One could easily see that tertiary alloys encompass a richer diversity of physical systems compared to binary systems. The introduction of new isoelectronic species and its compositional variation generates material systems with a broad spectrum of properties. The following are a few properties influenced and tuned by isoelectronic compositional variation.

- Structural parameters like lattice parameters and crystallinity.
- Optoelectronic parameters like bandgap, spin–orbit splitting energy, and the temperature sensitivity of bandgap.
- Transport properties like doping, electron–hole mobility.

Bandgap and lattice engineering of isoelectronic III–V alloys pushes its applicability to the fabrication of hybrid solar cells, LEDs, and lasers [13–15].

The strong influence of isoelectronic alloying on the structural, optoelectronic, and transport properties would inevitably modify the terahertz emission properties also.

4 III–V Bismide Alloys

Bismuth is the heaviest stable member in group V. Bismuth sets itself apart from the rest of the members with its highest atomic radius and lowest electronegativity. It acts as an isoelectronic substituent in III–V semiconductor systems. Bismuth incorporation into many of these III–V systems brings distinct modifications to the host semiconductors. Many of these characteristics have potential applications in the fabrication of optoelectronic devices ranging from detectors to solar cells and lasers. Some of the critical modifications introduced by Bi incorporation in III–V systems are discussed below.

5 Structural Properties

Lattice constant: Bismuth is the largest member of group V with an atomic radius of 230 pm. The anionic substitution of Bi necessarily leads to lattice expansion in general due to the high lattice mismatch. X-ray diffraction studies have revealed a definite shift in the characteristic peaks [16–18]. The studies have shown a monotonic increase in lattice constant with increasing Bi content in the case of GaAs. The lattice parameter data obtained from the XRD technique is often used to assess the Bi content in the alloy with the help of Vegard's law.

Crystallinity: The researchers always struggle with creating highly crystalline bismide alloys with large bismuth content. The anion mismatch is one of the important reasons, and the lattice expansion makes it difficult to achieve a lattice matching with the substrate [19].

6 Optoelectronic Properties

Bandgap: At dilute concentrations, Ga containing III–V: Bi alloys display a linear decrease in the bandgap [20]. In the case of $GaSb_{1-y}Bi_y$, the reduction happens at a rate of 30–40 meV/% of Bi [21, 22]. As the disparity between the anions increases, as in the case of the $GaAs_{1-x}Bi_x$ system, the bandgap drop is more pronounced and happens at a rate of ~80–90 meV/% of Bi [18, 23–26]. Many theoretical approaches have predicted bandgap bowing effects in III–V systems. Quantum dielectric theory [27], tight-binding method [28], DFT [22], virtual crystal approximation (VCA) [27], band anticrossing model (BAC) [29], etc., are the main theoretical approaches used to model the bandgap reduction with Bi incorporation in III–V semiconductors. Out of these, the BAC model fits well with the GaAsBi system, and a combination of BAC and VCA models provides a satisfactory explanation for the observed bandgap reduction in GaSbBi (Fig. 2).

Large spin–orbit splitting energy: The large spin–orbit splitting in III–V semiconductors doped with bismuth is also due to valance band anticrossing. The interaction of electron spin–orbital angular momentum with heavy Bi atom leads to the shift of the spin–orbit band of the new system to lower energy. This phenomenon, along with the movement of the valance band to higher energy, results in large spin–orbit splitting [24, 26, 33]. Such effects are useful for applications in spintronics.

7 Transport Properties

Unintentional doping: Bi-related states appear close to the valence band maxima of the host semiconductor, which in turn mainly affects the hole transport in the bismide alloys. One of the most crucial characteristics in all the gallium-containing

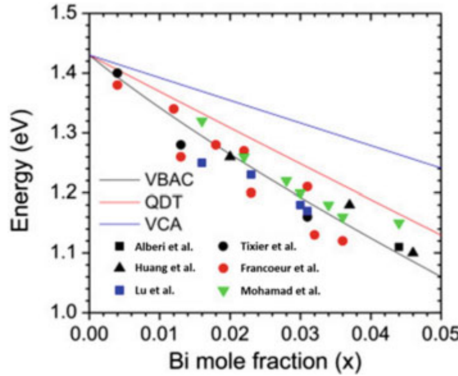

Fig. 2 Bandgap (E_g) reduction in GaAsBi observed from various studies reported in references [18, 23, 26, 30–32]. The figure also shows the comparison of experimental results to the theoretical calculations based on valance band anticrossing (VBAC), quantum dielectric theory (QDT), and virtual crystal approximation (VCA) [27]

III–V bismides is the introduction of the unintentional *p*-type character. The *p*-nature arises due to the formation of acceptor-like states induced by Bi, whose concentration increases at higher Bi content. One of the possible explanations for the acceptor states comes from the ability of Bi to have a valency of 3 as in Bi_2Te_3 or Bi_2Se_3 [34]. The valency of 3 comes as a consequence of large energy separation between $6s^2$ and $6p^3$ atomic orbitals in a heavy atom like Bi. A small fraction of Bi remains like this in the bismide alloys. In such a scenario, Bi can act as a double acceptor when residing in group V sub-lattice. Hence, a higher Bi concentration could lead to a higher hole density. An alternate route to explain the increased *p*-nature is the fact that Bi shifts the valence band edge to higher energies, closer to Fermi-level stabilization energy. The reduced activation energy favors the formation of acceptor-like defect states. This effect is observed in many bismide alloys, including GaAsBi [35–37] and GaSbBi [38, 39] (Fig. 3).

Hole mobility: The hole mobility shows remarkable degradation with Bi incorporation [35, 36, 40, 41]. The decrease in hole mobility is due to increased scattering rate by isolated as well as clustered Bi atoms. These sites could act as potential well for holes. Along with the drop in hole mobility, there is an increase in carrier effective mass with increasing Bi content in the alloy. This effect happens due to the strong hybridization of Bi-related levels with the host's VB. In short, the perturbation of Bi on CB is much weaker than that on VB, and consequently, the mobility of the electron is less affected compared to holes.

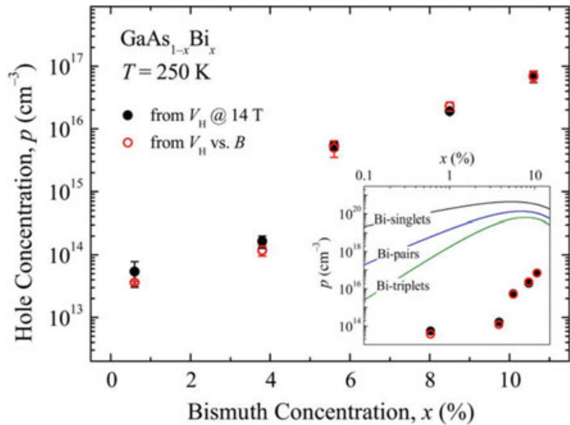

Fig. 3 Increase in the hole concentration in $GaAs_{1-x}Bi_x$ with increasing Bi content (x) observed by Pettinari et al. in reference [36]

8 Terahertz Emission from III–V-Bismide Alloys

As mentioned already, terahertz emission is a complex phenomenon influenced by a plethora of factors. Isoelectronic alloying could allow us to tweak many of these factors and alter the terahertz emission properties in semiconductors. In the previous section, we have discussed the characteristic deviation of bismide alloys from the parent III–V system. The material characteristics like bandgap, doping, and mobility have a crucial role in the terahertz emission phenomenon. In the following sections, we shall discuss the terahertz emission mechanisms in the GaAsBi and GaSbBi systems.

9 GaAsBi

Much investigation has been done on THz emission aspects of GaAs [5, 42]. With typical NIR excitation wavelengths and moderate excitation densities (~mJ/cm^2), the primary THz emission mechanism is surface field-assisted transient currents. GaAs being a wide-bandgap semiconductor, the system offers the possibility of considerable band bending and high built-in surface fields. The influence of the photo–Dember effect is minimal in GaAs when photoexcited at wavelengths close to the bandgap. These facts have been verified very well over the last couple of decades, and there is a consensus regarding this among researchers. However, in GaAs, excitation with high-energy photons results in a shift to photo–Dember emission. The reason for this is higher carrier temperature due to higher excess kinetic energy [4]. In addition to transient currents, the nonlinear phenomenon of optical rectification is also prevalent in GaAs [42].

In this section, we shall discuss the terahertz emission emerging out of nonlinear phenomena and transient currents in GaAsBi. One must keep in mind that both these emission phenomena are present in the GaAs system as well.

9.1 Optical Rectification

The terahertz emission from GaAsBi due to 800 nm excitation with moderate fluences shows a very clear indication of OR. An essential characteristic of the NL processes is the strong dependence of THz emission on the relative orientation of the excitation laser polarization and the crystal axes. For instance, in a zinc-blende structure, following relations dictate the dependence of *p*-polarized THz emission on the azimuthal angle (ϕ) with *p*-polarized laser excitation, due to bulk OR [43].

$$\begin{aligned} E_{p-p}^{\langle 100\rangle} &\approx \cos 2\phi \\ E_{p-p}^{\langle 110\rangle} &\approx \sin\phi + \sin 3\phi \\ E_{p-p}^{\langle 111\rangle} &\approx a + b\cos 3\phi \end{aligned} \tag{2}$$

The surface field-assisted OR has a different set of rules for azimuthal dependence. The studies so far have looked at the epilayers grown on the <100> and <311>B substrates. The GaAsBi epilayers grown on (311)B face has a rather interesting azimuthal dependence [44]. The bare <311>B GaAs substrate and the GaAsBi epilayers show entirely different trends in terahertz emission with azimuthal rotation. With the careful analysis of the second- and third-order susceptibility tensor in zinc-blende crystals, one could, in principle, arrive at the azimuthal dependence for any crystal plane. In doing so, the azimuthal dependence from (311)B GaAs substrate agrees well with that of bulk OR. While the trends in epilayer differed significantly, this could well be explained by considering a combination of bulk as well as surface field-assisted OR [44].

The surface field-assisted OR phenomenon arises due to the presence of a static electric field in the zinc-blende structure. Such a static electric field can be present on the surface of semiconductors, as discussed earlier. In such cases, $\left(\text{say, } E_z^{\text{surf}} \neq 0\right)$ the third-order nonlinearity $\left(\chi_{ijkz}^{\{3\}}\right)$ can contribute to an effective second-order nonlinearity, as expressed below.

$$\chi_{ijk}^{\{2\}\text{eff}} = \chi_{ijk}^{\{2\}\text{bulk}} + 3\chi_{ijkz}^{\{3\}} E_z^{\text{surf}} \tag{3}$$

While the (311)B-grown GaAsBi layers show terahertz emission via bulk and surface OR, studies have shown no evidence of surface OR contribution in the case of (100) grown GaAsBi epilayers. Also, in (100) orientation, zinc-blende structures show no azimuthal dependence in the case of surface OR (Fig. 4).

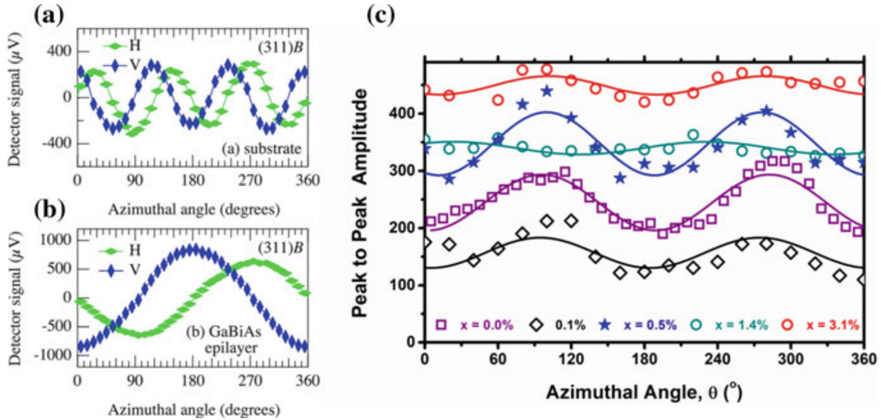

Fig. 4 Azimuthal angle dependence of THz emission from **(a)** GaAs (311)B substrate and **(b)** GaAsBi epilayer reported in reference [44]. **(c)** Similar azimuthal dependence from (100) GaAsBi epilayer reported in reference [45]

Studies have shown that the nonlinear phenomenon gets weaker with increasing Bi content in the alloy [45]. The reason is not entirely apparent yet. The Bi-induced bandgap bowing might also help us partially to explain the reduction in the contribution of OR. With increased optical absorption at lowered bandgap, the electron–hole pair generation process readily consumes the excitation photons. Hence, a lesser number of photons are available for nonlinear processes, which reduces the THz emission via OR. The effect of Bi alloying on the nonlinear susceptibility (nonlinear coefficients) is so far not known.

9.2 Transient Photocurrents

As mentioned earlier, transient currents are the dominant mechanism when it comes to THz emission in GaAs at 800 nm excitation, at low to moderate fluences. Studies show similar behavior in the case of GaAsBi systems too. The transient current could be due to the surface field or photo–Dember effect, depending on several factors. The extent of bismuth concentration itself is one of the most critical factors. At low bismuth content, the GaAsBi system is predominantly a surface field emitter, just like GaAs. Such behavior is easily understandable, considering the high-bandgap semiconductor system. One would see that the polarity of THz signals from *p*- and *n*-doped GaAsBi is opposite to each other. With increasing Bi content, the bandgap of the alloy system linearly decreases. Consider two semiconductors with different bandgaps, which are excited with radiation at the same wavelength (above bandgap excitation). Then, the carriers in the semiconductor with lower bandgap would have higher excess energy (and carrier temperature). Such a situation is very favorable

for creating diffusion current. Hence, decreasing the bandgap by incorporating more and more Bi makes the photo–Dember effect increasingly favorable (Fig. 5).

We reported such a transition happening somewhere between x ~ 0.5% and 1.4% Bi [45]. In the study, all the samples in the set ($0 \leq x \leq 3.1\%$) had inherited p-type doping associated with Bi incorporation. The THz pulses showed opposite polarity between 0.5 and 1.4% due to a crossover in the emission mechanism from

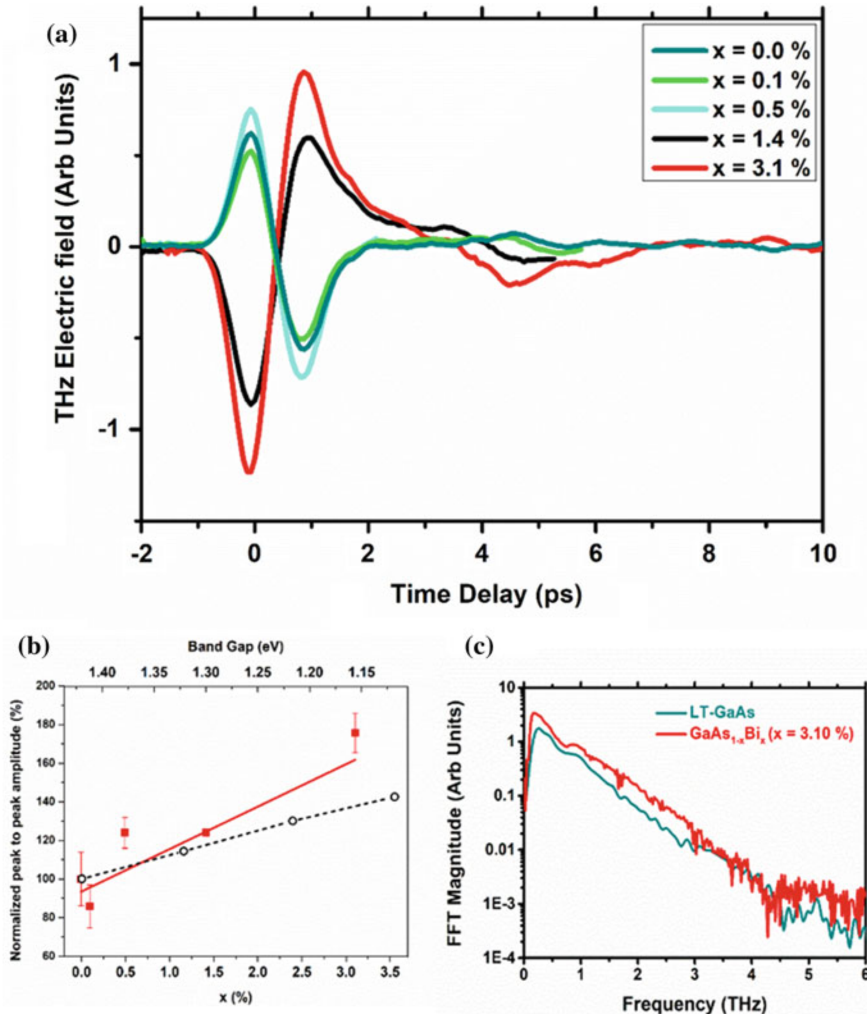

Fig. 5 THz emission characteristics of (100) $GaA_{1-x}Bi_x$ epilayers observed in reference [45]. **(a)** Comparison of THz pulses obtained from epilayers of varying Bi content under similar experimental conditions. One could see the polarity reversal in THz emission between $x \approx 0.5$ and 1.4%. **(b)** Trends in THz emission with varying Bi content and its comparison to the theoretical prediction in reference [46]. **(c)** The broadband emission spectrum from bismide alloys

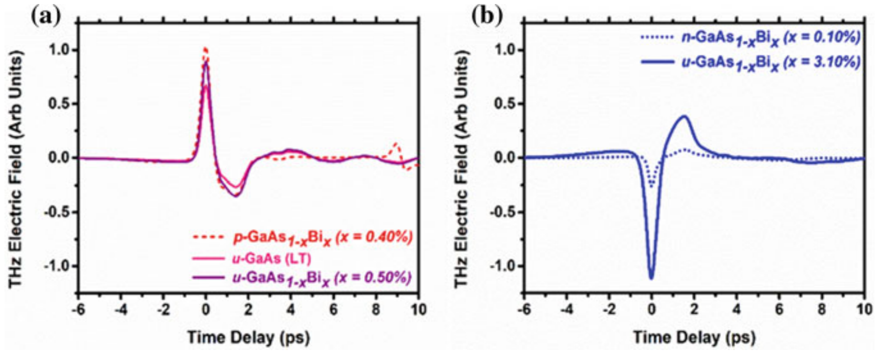

Fig. 6 **(a)**, **(b)** compare the THz pulse polarities of unintentionally doped (u) alloys to the *n*- and *p*-doped GaAsBi alloys. At low Bi concentration, the emission is dominated by drift currents. The claim is supported by the opposite polarity of the THz pulse in *n*- and *p*-type GaAsBi samples

surface field-assisted emission to photo–Dember dominated emission. One could see that with 1.55 eV (800 nm) excitation even at $x \sim 1.4\%$, the carriers would have around twice the excess energy compared to that in GaAs. The *p*-doping density in $GaAs_{1-x}Bi_x$ with increasing x could have a positive impact on the surface field and THz emission. However, in the above study, that effect is seen to be overshadowed by the increase of the photo-Dember effect. In the above study, there is an enhancement in the terahertz emission amplitude with increasing Bi content too. However, the terahertz emission could also face a backlash due to the reduced transport quality by bismuth induced defects [47] (Fig. 6).

The dominance of the photo–Dember effect becomes pronounced in the GaAsBi system with increasing excitation photon energy. But the photo–Dember current does not increase indefinitely with photon energy. The emission efficiency starts to drop once the excess energy of carriers crosses the energy difference between the Γ valley and satellite valley [47]. In such cases, the carriers start to scatter to the higher energy, low-mobility conduction band valleys. This reduces the photo–Dember efficiency. This technique is useful in finding the position of satellite valleys in the new $GaAs_{1-x}Bi_x$ alloys.

9.3 Photoconductive Antennas

GaAs is used extensively for the fabrication of THz photoconductive antenna, making it extremely relevant in THz sciences. Semi-insulating (SI) and low-temperature grown (LT) GaAs substrates are the most used photoconductive materials [48]. LT-GaAs, in particular, is the best material for making high-amplitude, broadband THz PCAs. The LT-GaAs has high resistivity, fast carrier decay, and low dark currents, which makes it ideal for PCA applications. One could also use cheaper SI-GaAs-based THz antennas for spectroscopic applications. If one intends to use a large

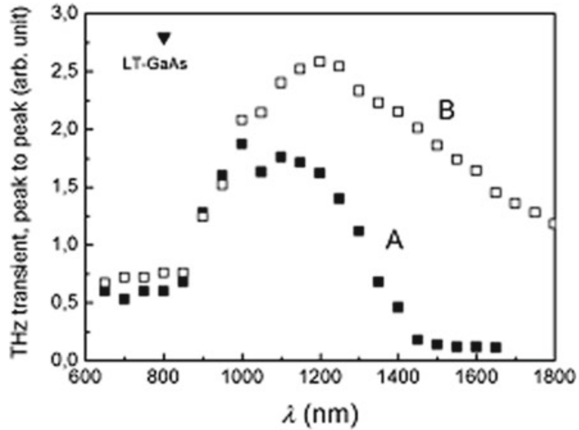

Fig. 7 Detection efficiency of GaAsBi-based PCAs which operate with long wavelength excitation [53]

aperture PCA emitter, SI-GaAs offers results comparable to LT-GaAs or often better [48, 49].

GaAsBi alloys also show great potential in PCA fabrication. The material also shows very fast carrier relaxation and high enough dark resistivity. GaAsBi PCAs operating at 800 nm are well known today [50–52]. But the most attractive prospect of GaAsBi-based PCAs lies in the bandgap tunability of the alloy. The bandgap bowing with Bi incorporation could lead to the usage of fiber lasers emitting in the 1–1.55 μm wavelength range for exciting the PCAs. Fiber lasers are far more compact and cheaper compared to the Ti-sapphire lasers that power GaAs-based PCAs. Arlauskus et al. have already demonstrated $GaAs_{1-x}Bi_x$-based PCAs with $x \sim 6\%$ being able to detect THz pulses even at excitation wavelengths as high as 1.8 μm [53]. Commercial GaAsBi PCAs are available now, which function in all-fiber mode operating at 1.06 μm. A shift to fiber laser-based THz spectroscopy systems could be a key to popularize the THz radiation and revolutionize its industrial applications (Fig. 7).

9.4 GaSbBi

GaSb is a low bandgap material with a bandgap $E_g \approx 0.72$eV. Surface fields do exist in GaSb; however, the strength is meager compared to GaAs due to the low bandgap of GaSb. The THz emission from GaSb due to surface field acceleration is much lower compared to GaAs. GaSb has a high absorption coefficient at typical Ti: Sapphire excitation wavelength ($\lambda \approx 800$nm; $E_{h\nu} \approx 1.55$ eV), and the carriers achieve high excess kinetic energy at such excitation conditions. One might be tempted to predict a stronger diffusion current due to the photo-Dember effect. However, there are more hurdles in GaSb for efficient diffusion currents driven THz emission. The satellite valleys of GaSb are very close to the Γ valley ($E_{\Gamma-L} \approx 0.084$eV and

$E_{\Gamma-X} \approx 0.31\text{eV}$). Excitation with well above bandgap radiation readily scatters the carriers to low mobility satellite valleys reducing the photocurrents and THz emission [7].

We looked at the impact of Bi incorporation on the THz emission. We reported a steady increase in THz emission with increasing Bi content in GaSbBi alloys grown via liquid phase epitaxy [54]. The bare GaSb, as mentioned earlier, is a weak THz emitter, with the emission intensity, which is only about 1/20th of that from LT-GaAs (Fig. 8). However, the emission amplitude from GaSbBi becomes comparable to that from LT-GaAs at a Bi content of ~1.65%. Bismuth incorporation in GaSb gives *p*-nature to the new alloy. As discussed earlier, studies have shown an increase in the *p*-doping density with increasing Bi content [38]. The study attributed the increased strength of the surface field due to increased doping density as the reason for such an emission enhancement. Another work on the GaSb system had revealed such an improvement in THz emission from GaSb due to impurity compensated *n*-doping due to tellurium inclusion [10]. The effect of bandgap lowering should not impact the photo–Dember effect so much at 1.55 eV excitation, as the GaSb system already has a low bandgap and excess carrier energy will not very different in the GaSbBi alloys with different Bi concentrations.

The study of the terahertz radiation pattern reveals the orientation of radiating dipole in the semiconductor system. We did this by rotating the sample with respect to the excitation beam (Fig. 9). The radiation pattern ($A^\circ(\theta_\mathrm{d})$) due to a dipole oriented at an angle X to the normal to the surface, inside the semiconductor is as follows [54].

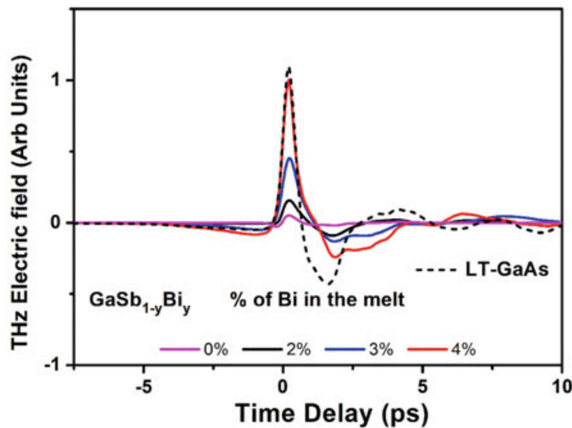

Fig. 8 THz pulses from GaSbBi alloys with varying Bi content and its comparison to LT-GaAs. The anionic Bi content in the alloy increases with increasing Bi content in the growth melt. The highest Bi content, in this case, is 1.65% Bi when grown at 4% Bi in the growth melt. The emission improves around 20-fold between GaSb and $\mathrm{GaS}_{1-y}\mathrm{Bi}_y$ ($y \approx 1.65\%$)

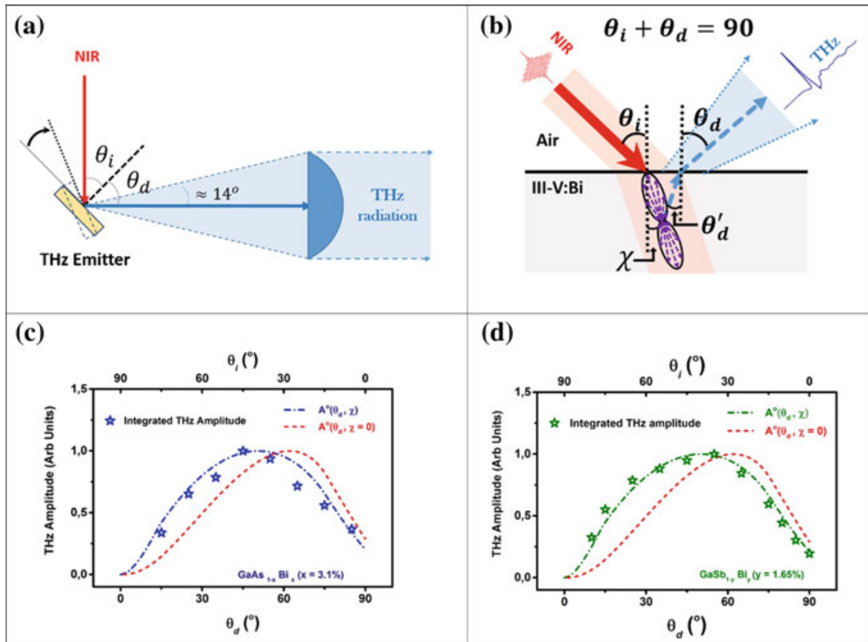

Fig. 9 **(a)** A schematic illustration of the experimental system for studying the dependence of THz emission on incidence/detection angle and, **(b)** the optical alignment of photocarriers in the semiconductor. The (time) integrated amplitude of the experimentally observed THz radiation from **(c)** $GaAs_{1-x}Bi_x$ and **(d)** $GaSb_{1-y}Bi_y$ emitter, along with the simulated pattern (with and without optical orientation) using Eq. 5 (dash-dotted line). Eq. 5 was integrated for $\theta_d \pm 14°$

$$A(\theta_d, \chi) \sim \frac{\cos\theta_d \times \sin\left(\theta_d' + \chi\right)}{\cos\theta_d' + n\cos\theta_d} \tag{4}$$

$$A^\circ(\theta_d, \chi) \propto [1 - R(90 - \theta_d)] \times \sin\theta_d \times A(\theta_d, \chi) \tag{5}$$

Our study on GaSbBi (and on GaAsBi) shows that the photocurrent (dipole) preferentially align along the refracted pump beam inside the III–V: Bi alloys. Such an "optical alignment" of carrier momentum points to the influence of the photo–Dember effect in the system. So far, no influence of optical rectification was observed from either GaSb or GaSbBi systems.

Further studies are required to understand the influence of Bi on the position of satellite valleys in GaSbBi alloys. Such influences could have a strong influence on the THz emission properties in the GaSbBi system.

To sum up, the terahertz emission from GaAsBi and GaSbBi could be enhanced with increasing Bi incorporation with 800 nm excitation. Giant bandgap bowing in GaAsBi leads to increased photocarrier temperature that enhances the photo–Dember effect in GaAsBi. The unintentional *p*-doping due to Bi inclusion strengthens the

surface field and hence the THz emission in GaSbBi. However, the bandgap bowing in GaSbBi and *p*-doping in GaAsBi seems to be of lesser influence in THz emission amplitude. However, the degradation of crystal quality will reduce the transport quality and the emission amplitude in any semiconductor system. It is exceptionally challenging to create good-quality alloys with high Bi content. But, if we succeed in that endeavor, it would be interesting to learn the THz emission phenomenon from high Bi content alloys with excellent crystal quality. The knowledge of THz emission dynamics in bismide alloys is still minimal. Further studies, including excitation spectra dependence, must be done on bismide systems of a wide composition range if we are to have a broader understanding of the subject.

9.5 Application in THz Spectroscopy

The THz emission from the GaSbBi and GaAsBi films is spectrally broad. The useful tail of the emission extends up to ~4.5 THz. The detected bandwidth could be limited because of the low sensitivity of the PCA detector at higher THz frequencies. We had compared the performance of the GaAsBi emitter and a commercially available iPCA in a THz-TDS system. The emission amplitude from GaAsBi or GaSbBi surface is several orders of magnitude lower compared to the iPCA, but its spectral reach surpasses that of a commercially available iPCA. We had used GaSbBi emitter to study the THz response of β BBO crystal and demonstrated that compared to a commercially available interdigitated PCA (iPCA), the frequency limit in which material response is faithfully measured is higher in the case of GaSbBi. Similar performance has also been obtained from GaAsBi. For example, as shown in Fig. 10, we compare the THz transmitted signal through a spin-ladder compound $\mathbf{Sr_{14}Cu_{24}O_{42}}$. This particular compound attenuates the transmission of THz signal in the frequency band from 0.25–1 THz, which results in two peaks (~0.25 THz and ~1 THz) in the

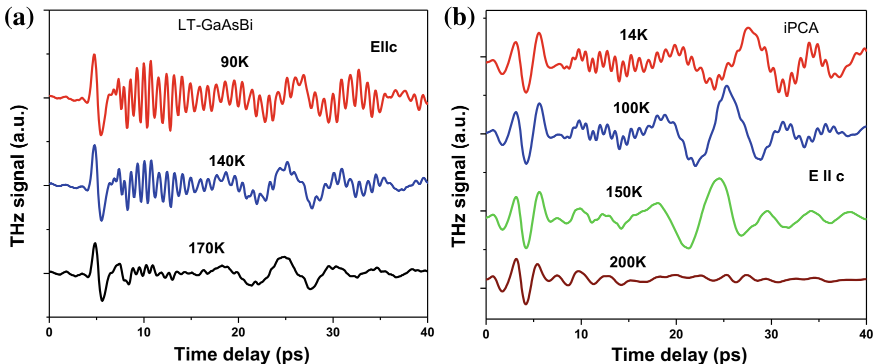

Fig. 10 **a** THz signal generated using an (**a**) GaAsBi emitter and **b** commercially available iPCA after transmitting through a $Sr_{14}Cu_{24}O_{42}$ crystal

transmitted spectra. These two peaks give rise to two kinds of oscillations, (i) a slow oscillation with a period of ~4 ps and (ii) a fast oscillation with a period of ~1 ps. As one can see, the fast oscillations are much more visible in the case of THz generation using GaAsBi compared to iPCA, due to the higher bandwidth of GaAsBi emitter. This demonstrates the feasibility of GaSbBi and GaAsBi alloy emitters for broadband THz-TDS applications.

References

1. R.W. Boyd, *Nonlinear Optics. Nonlinear Optics*. Elsevier Inc. (2008)
2. R.B. Darling, Defect-state occupation, fermi-level pinning, and illumination effects on free semiconductor surfaces. Phys. Rev. B. **43**(5), 4071–4083 (1991)
3. W.H. Brattain, J. Bardeen, Surface properties of germanium. Am. Teleph. Telegr. Co. **32**, 1 (1952)
4. J.N. Heyman, N. Coates, A. Reinhardt, G. Strasser, Diffusion and drift in terahertz emission at GaAs surfaces. Appl. Phys. Lett. **83**(26), 5476–5548 (2003)
5. X.C. Zhang, J. Xu, *Introduction to THz Wave Photonics, Introduction to THz Wave Photonics* (Springer, US, 2010), pp. 1–246
6. A. Arlauskas, A. Krotkus, THz excitation spectra of AIIIBV semiconductors. Semicond. Sci. Technol. **27**, 115015 (2012)
7. P. Gu, M. Tani, S. Kono, K. Sakai, X.C. Zhang, Study of terahertz radiation from InAs and InSb. J. Appl. Phys. **91**(9), 5533–5537 (2002)
8. I. Wilke, R. Ascazubi, H. Lu, W.J. Schaff, Terahertz emission from silicon and magnesium doped indium nitride. Appl. Phys. Lett. **93**(22), 22113 (2008)
9. R. Ascazubi, I. Wilke, K.J. Kim, P. Dutta, Terahertz emission from $Ga_{1-x}In_xSb$. Phys. Rev. B. **74**, 075323 (2006)
10. R. Ascázubi, C. Shneider, I. Wilke, R. Pino, P.S. Dutta, Enhanced terahertz emission from impurity compensated GaSb. Phys. Rev. B—Condens. Matter. Mater. Phys. **72**(4), 045328 (2005)
11. S. Kono, P. Gu, M. Tani, K. Sakai, Temperature dependence of terahertz radiation from *n*-type InSb and *n*-type InAs surfaces. Appl. Phys. B Lasers Opt. **71**(6), 901–904 (2000)
12. R. Adomavičius, A. Urbanowicz, G. Molis, A. Krotkus, E. Šatkovskis, Terahertz emission from p-InAs due to the instantaneous polarization. Appl. Phys. Lett. **85**(13), 2463–2465 (2004)
13. Wang L, Zhang L, Yue L, Liang D, Chen X, Li Y, et al. Novel dilute bismide, epitaxy, physical properties and device application. Crystals [Internet]. 7(3):63 (2017). Available from http://www.mdpi.com/2073-4352/7/3/63
14. R.F. Davis, III–V nitrides for electronic and optoelectronic applications. Proc. IEEE **79**(5), 702–712 (1991)
15. I. Marko, S.J. Sweeney, Progress towards III–V-bismide alloys for near- and mid-infrared laser diodes. IEEE J. Sel. Top. Quantum Electron. **23**(6), 150512 (2017)
16. K. Oe, H. Okamoto, New semiconductor alloy $GaAs_{1-x}Bi_x$ grown by metal organic vapor phase epitaxy. Jpn. J. Appl. Phys. **37**(11), 1283–1285 (1998)
17. Y. Takehara, M. Yoshimoto, W. Huang, J. Saraie, O.E. Kunishige, A. Chayahara et al., Lattice distortion of GaAsBi alloy grown on GaAs by molecular beam epitaxy. Japan. J. Appl. Phys. Part 1 **45**(1A), 67–69 (2006)
18. S. Tixier, M. Adamcyk, T. Tiedje, S. Francoeur, A. Mascarenhas, P. Wei et al., Molecular beam epitaxy growth of $GaAs_{1-x}Bi_x$. Appl. Phys. Lett. **82**(14), 2245–2247 (2003)
19. K.M. Yu, S.V. Novikov, R. Broesler, A.X. Levander, Z. Liliental-Weber, F. Luckert et al., GaNAs alloys over the whole composition range grown on crystalline and amorphous substrates. Phys. Status Solidi. Curr. Top Solid State Phys. **8**(7–8), 2503–2505 (2011)

20. M.P. Polak, P. Scharoch, R. Kudrawiec, First-principles calculations of bismuth induced changes in the band structure of dilute Ga–V–Bi and In–V–Bi alloys: Chemical trends versus experimental data. Semicond Sci Technol. **30**(9), 094001 (2015)
21. M.K. Rajpalke, W.M. Linhart, M. Birkett, K.M. Yu, D.O. Scanlon, J. Buckeridge et al., Growth and properties of GaSbBi alloys. Appl. Phys. Lett. **103**, 142106 (2013)
22. M.P. Polak, P. Scharoch, R. Kudrawiec, J. Kopaczek, M.J. Winiarsky, W.M. Linhart et al., Theoretical and experimental studies of electronic band structure for $GaAs_{1-x}Bi_x$. J. Phys. D Appl. Phys. **47**, 355107 (2014)
23. S. Francoeur, M.-J. Seong, A. Mascarenhas, S. Tixier, M. Adamcyk, T. Tiedje, Band gap of $GaAs_{1-x}Bi_x$, 0 < x < 3.6%. Appl. Phys. Lett. **82**, 3874 (2003)
24. Z. Batool, K. Hild, T.J.C. Hosea, X. Lu, T. Tiedje, S.J. Sweeney, The electronic band structure of GaBiAs/GaAs layers: influence of strain and band anti-crossing. J. Appl. Phys. **111**, 113108 (2012)
25. J. Yoshida, T. Kita, O. Wada, K. Oe, Temperature dependence of $GaAs_{1-x}Bi_x$ band gap studied by photoreflectance spectroscopy. Japanese J Appl Physics, Part 1 **42A**(2), 371–374 (2003)
26. K. Alberi, O.D.D. Walukiewicz, K.M.Y. Bertulis, A. Krotkus, Valence band anticrossing in $GaBi_xAs_{1-x}$. Appl. Phys. Lett. **91**, 051909 (2007)
27. D.P. Samajdar, S. Dhar, Estimation of Bi induced changes in the direct E_0 band gap of III–V-Bi alloys and comparison with experimental data. Phys. B **484**, 27–30 (2016)
28. M. Usman, C.A. Broderick, A. Lindsay, E.P. O'Reilly, Tight-binding analysis of the electronic structure of dilute bismide alloys of GaP and GaAs. Phys. Rev. B. **84**, 245202 (2011)
29. K. Alberi, J. Wu, W. Walukiewicz, K.M. Yu, O.D. Dubon, S.P. Watkins et al., Valence-band anticrossing in mismatched III–V semiconductor alloys. Phys. Rev. B. **75**, 045203 (2007)
30. W. Huang, K. Oe, G. Feng, M. Yoshimoto, Molecular-beam epitaxy and characteristics of Ga $N_yAs_{1-x-y}Bi_x$. J Appl Phys. **98**(5), 053505 (2005)
31. X. Lu, D.A. Beaton, R.B. Lewis, T. Tiedje, Y. Zhang, Composition dependence of photoluminescence of $GaAs_{1-x}Bi_x$ alloys. Appl. Phys. Lett. **95**(4), 2007–2010 (2009)
32. A.R. Mohmad, F. Bastiman, C.J. Hunter, R.D. Richards, S.J. Sweeney, J.S. Ng et al., Localization effects and band gap of GaAsBi alloys. Phys. Status Solidi. Basic Res. **251**(6), 1276–1281 (2014)
33. B. Fluegel, S. Francoeur, A. Mascarenhas, S. Tixier, E.C. Young, T. Tiedje, Giant spin-orbit bowing in $GaAs_{1-x}Bi_x$. Phys. Rev. Lett. **97**(6), 11–14 (2006)
34. H.X. Deng, J. Li, S.S. Li, H. Peng, J.B. Xia, L.W. Wang et al., Band crossing in isovalent semiconductor alloys with large size mismatch: First-principles calculations of the electronic structure of Bi and N incorporated GaAs. Phys. Rev. B—Condens. Matter. Mater. Phys. **82**(19), 4–7 (2010)
35. S. Nargelas, K. Jarašiunas, K. Bertulis, V. Pačebutas, Hole diffusivity in GaAsBi alloys measured by a picosecond transient grating technique. Appl. Phys. Lett. **98**(8), 082115 (2011)
36. G. Pettinari, A. Patanè, A. Polimeni, M. Capizzi, X. Lu, T. Tiedje, Bi-induced *p*-type conductivity in nominally undoped Ga(AsBi). Appl. Phys. Lett. **100**(9), 092109 (2012)
37. G. Pettinari, H. Engelkamp, P.C.M. Christianen, J.C. Maan, A. Polimeni, M. Capizzi et al., Compositional evolution of Bi-induced acceptor states in $GaAs_{1-x}Bi_x$ alloy. Phys. Rev. B. **83**, 201201(R) (2011)
38. N. Segercrantz, J. Slotte, I. Makkonen, F. Tuomisto, I.C. Sandall, M.J. Ashwin et al., Hole density and acceptor-type defects in MBE-grown $GaSb_{1-x}Bi_x$. J. Phys. D Appl. Phys. **50**, 295102 (2017)
39. J. Kopaczek, R. Kudrawiec, W. Linhart, M. Rajpalke, T. Jones, M. Ashwin et al., Low- and high-energy photoluminescence from $GaSb_{1-x}Bi_x$ with $0 < x < 0.042$. Appl. Phys. Expr. **7**, 111202 (2014)
40. D.A. Beaton, R.B. Lewis, M. Masnadi-Shirazi, T. Tiedje, Temperature dependence of hole mobility in $GaAs_{1-x}Bi_x$ alloys. J. Appl. Phys. **108**, 083708 (2010)
41. R.N. Kini, A.J. Ptak, B. Fluegel, R. France, R.C. Reedy, A. Mascarenhas, Effect of Bi alloying on the hole transport in the dilute bismide alloy $GaAs_{1-x}Bi_x$. Phys. Rev. B. **83**, 075307 (2011)

42. S.L. Dexheimer, *Terahertz spectroscopy: principles and applications, principles and applications* (CRC Press, Terahertz Spectroscopy, 2017), pp. 1–331
43. M. Reid, I.V. Cravetchi, R. Fedosejevs, Terahertz radiation and second-harmonic generation from InAs: bulk versus surface electric-field-induced contributions. Phys. Rev. B. **72**, 035201 (2005)
44. K. Radhanpura, S. Hargreaves, R.A. Lewis, M. Henini, The role of optical rectification in the generation of terahertz radiation from GaBiAs. Appl. Phys. Lett. **94**, 251115 (2009)
45. C.P. Vaisakh, A. Mascarenhas, R.N. Kini, THz generation mechanisms in the semiconductor alloy, $GaAs_{1-x}Bi_x$. J. Appl. Phys. **118**, 165702 (2015)
46. D.L. Cortie, R.A. Lewis, The importance of scattering, surface potential, and vanguard counter-potential in terahertz emission from gallium arsenide. Appl. Phys. Lett. **100**, 261601 (2012)
47. V. Pačebutas, S. Stanionytė, A. Arlauskas, R. Norkus, R. Butkutė, A. Geižutis et al., Terahertz excitation spectra of GaAsBi alloys. J. Phys. D Appl. Phys. **51**, 474001 (2018)
48. N.M. Burford, M.O. El-Shenawee, Review of terahertz photoconductive antenna technology. Opt. Eng. **56**, 010901 (2017)
49. M. Tani, S. Matsuura, K. Sakai, S. Nakashima, Emission characteristics of photoconductive antennas based on low-temperature-grown GaAs and semi-insulating GaAs. Appl. Opt. **36**(30), 7853 (1997)
50. B. Heshmat, M. Masnadi-Shirazi, R.B. Lewis, J. Zhang, T. Tiedje, R. Gordon et al., Enhanced terahertz bandwidth and power from GaAsBi-based sources. Adv. Opt. Mater. **1**(10), 714–719 (2013)
51. K. Bertulis, A. Krotkus, G. Aleksejenko, V. Pačebutas, R. Adomavičius, G. Molis et al., GaBiAs: a material for optoelectronic terahertz devices. Appl. Phys. Lett. **88**(20), 201112 (2006)
52. V. Pačebutas, A. Bičiũnas, S. Balakauskas, A. Krotkus, G. Andriukaitis, D. Lorenc et al., Terahertz time-domain-spectroscopy system based on femtosecond Yb: fiber laser and GaBiAs photoconducting components. Appl. Phys. Lett. **97**, 031111 (2010)
53. A. Arlauskas, P. Svidovsky, K. Bertulis, R. Adomavičius, A. Krotkus, GaAsBi photoconductive terahertz detector sensitivity at long excitation wavelengths. Appl. Phys. Expr. **5**, 022601 (2012)
54. C.P. Vaisakh, M.K. Bhowal, S. Dhar, R.N. Kini, Enhanced terahertz emission from Bi incorporated GaSb. J. Phys. D Appl. Phys. **51**, 065112 (2018)